www.czasopisma.pan.pl PAN POLSKA AKADEMIA NAUK www.journals.pan.pl

Arch. Metall. Mater. **67** (2022), 4, 1209-1216

DOI: https://doi.org/10.24425/amm.2022.141044

ZHOULING LONG[1], HAIYANG LANG[2], JUN OU[2,3*]

EFFECT OF TIN ADDITION ON THE DEGRADABILITY AND CORROSION PROPERTIES OF A NEW Zn-1.0 WT.% Mg ALLOY

In this study, to investigate effects of tin addition on the microstructures and corrosion properties, Zn-1Mg-xSn (x = 1.0, 2.0 and 5.0 wt.%) ternary zinc alloys were prepared. The experimental results indicated that the Zn-1Mg-2.0 wt.% Sn alloy has the better mechanical properties compared with pure zinc and Zn-1Mg alloy. The tensile strength of the alloy material is 173.2±3.7 MPa, the yield strength is 120.7±2.4 MPa, the elongation is 5.64±0.08% and the hardness is 76.9±0.8 HV. The average degradation rate of the alloys immersion in SBF solution for 60 days is 0.16±0.03 mm/year, and the Zn-1Mg-2.0 wt.% Sn alloy hemolysis rate is only 0.81±0.02%. It is confirmed that the addition of tin is effective to improve the mechanical properties and degradation of Zn-1Mg alloy. It may be a candidate of the clinical application requirements of the degradable implant materials in orthopedics.

Keywords: Zn-1Mg alloy; Mechanical and corrosion properties; Degradability; Hemolysis rate

1. Introduction

With the development of society, there are millions of people with fracture problems caused by accidents such as car accidents or natural disasters every year, and it is showing an upward trend year by year [1]. At present, the most common method for clinical treatment of fractures is to implant artificial bone implants, such as titanium alloy, stainless steel, cobalt-chromium alloy, etc. [2-5]. Since the implantable material cannot exist in the human body for a long time, a second operation is required to remove it from the human body, which not only increases the economic burden, but also increases the postoperative risk of the patient [6,7]. Therefore, the advantages of biodegradable biomedical metal materials have received extensive attention from academia [8-10]. The biodegradable metal materials currently studied are mainly divided into three categories: magnesium alloys, iron alloys and zinc alloys [8,11,12].

In recent years, Zn-Mg alloy has received extensive attention in the field of biomedicine due to its good mechanical properties and biocompatibility. Zinc has a hexagonal close-packed (HCP) structure and is used to make several alloys due to its galvanizing and sacrificial properties [13]. Galvanic corrosion was observed in all binary Zn alloys with intermetallic phases. Zn acted as the anode in Zn-Fe [14], Zn-Cu [15], and Zn-Ag [16] alloys while Zn was the cathode in other alloys. Tang et al. [17] added Cu and Mg to pure Zn for alloying treatment, which improved the mechanical properties of pure Zn, and the corrosion rate met the requirements of biodegradable biomedical materials, and at the same time increased the cell proliferation rate. Li et al. [18] implanted zinc alloy into the bone marrow cavity of mouse femur. The experimental results showed that zinc alloy meets the degradation rate requirements of orthopedic repair implant materials, and an appropriate Zn^{2+} concentration can promote the formation of new bone. Bowen et al. [19] implanted pure zinc into the abdominal aorta of mice. The experimental results showed that Zn can reduce the incidence of cardiovascular stenosis. For zinc alloy research, there are Zn-Mg [20] and Zn-Li [21-23]. For bone implant zinc alloy research, there are now three types: Zn-Mg [24], Zn-Ca and Zn-Sr [18] reported. There are other elements beneficial to bone health as additional elements for research, such as Mn [25], Fe [14], Cu [15], Ag [16] and so on.

Tin has a low melting point, does not easily react with air and water at room temperature, has good ductility, has no physiological toxicity, and has a good sterilization effect. At the same time, the tin element is also an essential trace element for the human body, participating in the synthesis of protein and nucleic

[1] MATERIALS SCIENCE AND ENGINEERING, GUILIN UNIVERSITY OF TECHNOLOGY, CHINA
[2] GUILIN UNIVERSITY OF TECHNOLOGY, COLLEGE OF MATERIALS SCIENCE AND ENGINEERING /DENTAL CLINIC AND EXPERIMENTAL CENTER OF MEDICAL SCIENCES, 12 JIANGAN ROAD, GUILIN, 541004, GUILIN, CHINA
[3] GUILIN MEDICAL UNIVERSITY, EXPERIMENTAL CENTER OF MEDICAL SCIENCES, 26, HUANCHEN ROAD GUILIN, 541002, GUILIN, CHINA

* Corresponding author: gloujun@glut.edu.cn

acid, and enhancing the internal environment of the human body the stability. Chen et al. [26] studied the Mg-Sn structure and the mechanical properties of the alloy, and the results showed that Sn can significantly refine the grains and improve the mechanical properties of the alloy. Zhao et al. [27] studied at the corrosion properties and biocompatibility of Mg-Sn alloy, and experiments proved that Mg-Sn alloy is expected to become a new orthopedic implant surgical material. The hardness value of Mg-5Sn [28] is only 35.2 HV. Although these studies show that the addition of Sn can improve the properties of pure Mg, there are still insufficient mechanical properties, and the hardness value is low. The above research results can show that zinc alloys have good biocompatibility and suitable corrosion rate, while tin has good physical properties and biocompatibility, provides a theoretical basis for the experimental study. By consulting the literature [29], it is found that Zn-Sn alloy has no solid solution and intermediate phase, Zn-Mg alloy has Mg_2Zn_{11} phase and $MgZn_2$ phase, and Mg-Sn alloy has Mg_2Sn phase. At the same time, it is found that Zn-1Mg alloy has the best mechanical properties among Zn-Mg [20] alloys. Admixing is a common practice in Zn-Mg alloys but to the authors best knowledge there is no investigation in literature on its effects on the microstructure and corrosion properties through added trace tin into Zn-Mg alloy. For these reasons, in this study, we investigated the effects of Sn addition on the mechanical properties, corrosion behavior, and blood compatibility of the as-casted Zn-1Mg-xSn (x = 1.0, 2.0 and 5.0 wt.%) alloys.

2. Experimental

The alloys used in this study had the nominal composition of Zn-1.0 wt.% Mg-xSn (x = 1.0, 2.0 and 5.0 wt.%). Pure zinc ingots (purity ≥ 99.95% wt.%), pure magnesium ingots (purity ≥ 99.98% wt.%) and tin ingots (purity ≥ 99.999% wt.%) were prepared as raw materials. The melt was held at 650-700°C for 25 minutes and then poured into a pre-heated graphite crucible mold (diameter 120×30×13 mm). The raw materials are put into a according to the mass ratio, and the preheating temperature is 300°C. During the melting process, high-purity argon (Ar) produced by Guilin Hongrun Gas is introduced to prevent the added magnesium ingot from being oxidized. The cooled alloy ingot is wrapped with aluminum foil paper at a temperature of 250-350°C for 5 hours, and then air-cooled to room temperature.

The microstructure of the alloy was observed by optical microscope (BMM-230BDV Shanghai Batu Instrument Co., Ltd.). An X-ray diffraction analyzer (XRD, X'Pert PRO, and the Netherlands Pana analytical Instruments) was used to analyze the phase composition of the studied alloy using Cu target Kα-ray radiation. A field emission scanning electron microscope and its auxiliary energy spectrometer (S-4800, Japanese high-tech company/Oxford company, UK) were used to observe the element distribution of the sample.

A Vickers hardness tester (VH-5, Shanghai Hengyi Precision Instrument Co., Ltd.) was used to test the hardness of the sample. The loading load is 100 N, the pressure holding time is 15 s, and each sample is hit with 9 points, whichever is the average value is used as the hardness value of the sample. The tensile test uses an electronic universal tensile testing machine (DDL200KN, Changchun Machinery Science Research Institute Co., Ltd.) to test the tensile properties of the sample material at room temperature, the tensile rate is set to 1 mm/min, and each sample takes 3 parallel samples and their average values were taken as the tensile properties test value of the sample. Scanning electron microscope (SEM) and energy spectrometer (EDS) were used to analyze the fracture morphology of the tensile specimen.

The electrochemical corrosion experiment uses an electrochemical workstation (CHI-760, Beijing Huaputian Technology Co., Ltd.) for testing. A standard three-electrode electrochemical system is adopted, with pure zinc and Zn-1.0 wt.% Mg-xSn (x = 1.0, 2.0 and 5.0 wt.%) as the working electrode (WE), the saturated calomel electrode as the reference electrode (RE), the platinum electrode as the counter electrode (CE), and the corrosive medium is 80 ml 37°C SBF [30] solution. The working area of the sample is 10×10 mm^2, the open circuit potential method (OCP ± 0.6) V is used as the polarization curve to scan test range, and the scan rate is 1 mV/s, repeat the test three times and take the average value as the final test result.

The simulated body fluid immersion experiment is tested in SBF solution at 37°C, using ASTMG31-72 standard. The immersion test time is 7 days, 15 days, 30 days and 60 days respectively. The corrosion products on the sample surface were cleaned with 200 g/L CrO_3 solution, and the samples after cleaning and drying were weighed with a 1/10000 electronic balance (CP114, Shanghai Oehouse Instrument Co., Ltd.) to calculate the corrosion rate of the samples. The corrosion morphology of the soaked samples was observed by scanning electron microscopy (SEM).

The blood compatibility experiment was carried out according to the ISO-10993-4:2017 standard. The optical density (Dt value) of the sample supernatant was measured with a grating type continuous wavelength microplate reader (infinite M200 PRO, Swiss TECAN), the test wavelength was 541 nm. The platelet rich plasma (PRP) material prepared from the blood of New Zealand white rabbits was taken, and the prepared platelet rich plasma (PRP) material was added to the surface of the sample, and its distribution and adhesion state were observed with a scanning electron microscope.

3. Result and discussion

Fig. 1 shows the XRD patterns of the as-casted Zn-1Mg-xSn alloys (x = 1.0, 2.0 and 5.0 wt.%). The XRD pattern showed a strong peak on the Zn phase. Peaks also observed there is no intermediate phase between Zn and Sn. There are also find that a small amount of $MgZn_2$ and Mg_2Zn_{11} phase are found to exist stably in the zinc rich ternary system [20]. Peaks also find there is Mg_2Sn intermediate phase present and with the increase of Sn content the diffraction peaks of Mg_2Sn phase are increasing. For the peak area of the Mg_2Sn phase, Zn-Mg-5.0 wt.% Sn is 2.5 times that of Zn-1Mg-1.0 wt.% Sn, and there is not much

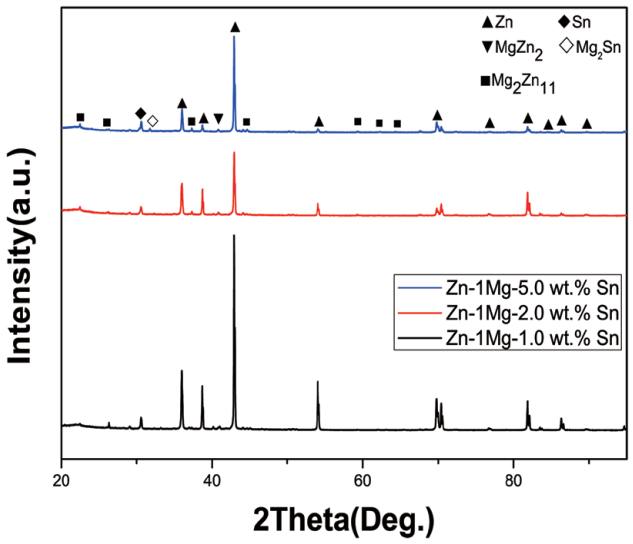

Fig. 1. X-ray diffraction energy spectrum of Zn-Mg-xSn alloys

difference between Zn-1Mg-1.0 wt.% Sn and Zn-1Mg-2.0 wt.% Sn. Therefore, it can be concluded that the prepared ternary alloy does not produce ternary solid solution.

Fig. 2 shows the optical microscope (OM) image and (EDS) image of the as-cast pure Zn and Zn-1Mg-xSn alloys. It can be seen from the figure that the grains of Zn-1Mg-xSn alloys are more obvious than those of pure zinc, and the grains are refined to a certain extent. The Zn-1Mg-xSn alloys sample was attached to the scanning electron microscope through the EDS energy spectrum analyzer of the Zn-1Mg-xSn alloys grain boundary. The experimental results show that the elements inside the crystal grains are Zn and Mg, indicating that Mg enters the crystal grains in the form of solid solution. The main elements at the grain boundaries are Zn, Mg and Sn. According to the analysis of OM, EDS and XRD patterns and conjunction with the literature [20], the precipitation of Mg_2Zn_{11} and $MgSn_2$ phases at the grain boundaries hinders the grain growth process

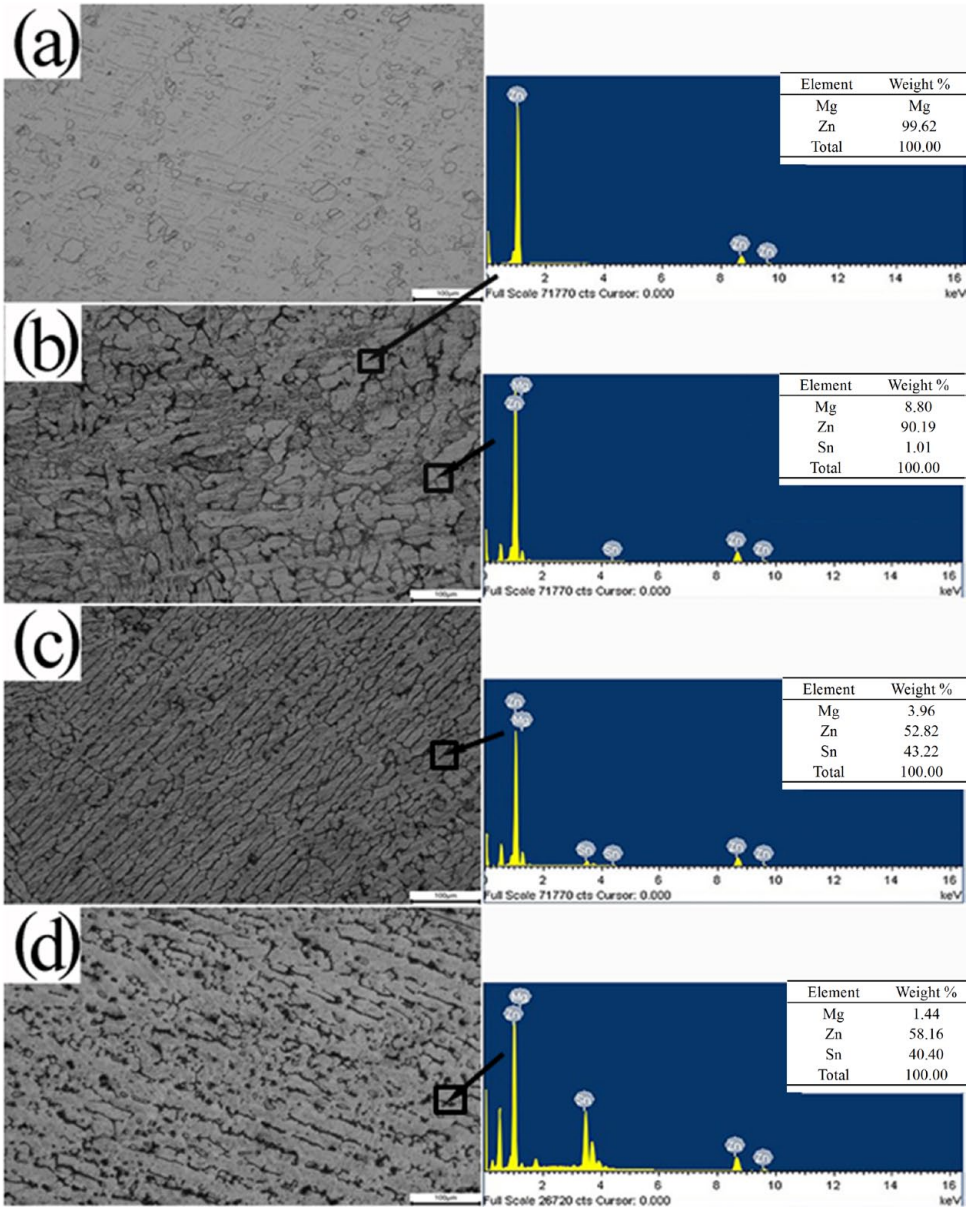

Fig. 2. As-cast metallographic microstructure and EDS: (a) Pure Zn; (b) Zn-1Mg-1.0 wt.% Sn; (c) Zn-1Mg-2.0 wt.% Sn; (d) Zn-1Mg-5.0 wt.% Sn

and refines the grains. Compared with pure zinc and Zn-1Mg, the metallographic structure of the Zn-1Mg-xSn alloys have been improved, and the grain size has been refined, because the Mg_2Zn_{11} phase and Mg_2Sn phase precipitated at the grain boundary hinder the solidification process the crystal grains grow, thereby increasing the number of crystal nucleation sites and benefited to alloys strengthener.

TABLE 1 shows the comprehensive mechanical properties of pure zinc, Zn-1Mg [31] and as-cast Zn-1Mg-xSn alloys. Compared with pure zinc and Zn-1Mg, the tensile strength (TS), yield strength (YS), microscopic hardness and elongation of Zn-1Mg-xSn alloys have been improved. The overall mechanical properties of Zn-1Mg-xSn alloys are on the rise, but with the increase of Sn content, the mechanical properties of the alloys first increase and then decrease. The improvement of mechanical properties of Zn-1Mg-xSn alloys is due to the presence of Mg_2Sn, $MgZn_2$ and Mg_2Zn_{11} phases in the alloy crystal, which leads to lattice distortion, impeding dislocation movement, increasing the difficulty of crystal slip, and improving the strength, toughness and hardness of the alloy. Meanwhile, Mg_2Sn phase is brittle phase. With the increase of Sn content, the elongation of Zn-Mg-xSn alloys has little change. Various mechanical properties show that the comprehensive mechanical properties of Zn-Mg-xSn alloys are good. Fig. 3 shows the tensile fracture

TABLE 1

Mechanical properties of pure zinc, Zn-1Mg-1.0 wt.% Sn, Zn-1Mg-2.0 wt.% Sn, Zn-1Mg-5.0 wt.% Sn

Materials (wt.%)	Tensile strength (MPa)	Yield strength (MPa)	Elongation (%)	Hardness (HV)
Pure Zn	31.5±1.0	22.4±0.5	0.87±0.02	28.0±0.2
Zn-1Mg-1.0 wt.% Sn	167.9±3.2	122.2±2.7	4.23±0.05	75.5±0.7
Zn-1Mg-2.0 wt.% Sn	173.2±3.7	120.7±2.4	5.64±0.08	76.9±0.8
Zn-1Mg-5.0 wt.% Sn	163.8±3.5	119.8±2.2	5.81±0.10	64.0±0.5
Zn-1Mg [31]	145.0±3.0	95.0±2.0	1.50±0.03	65.0±0.5

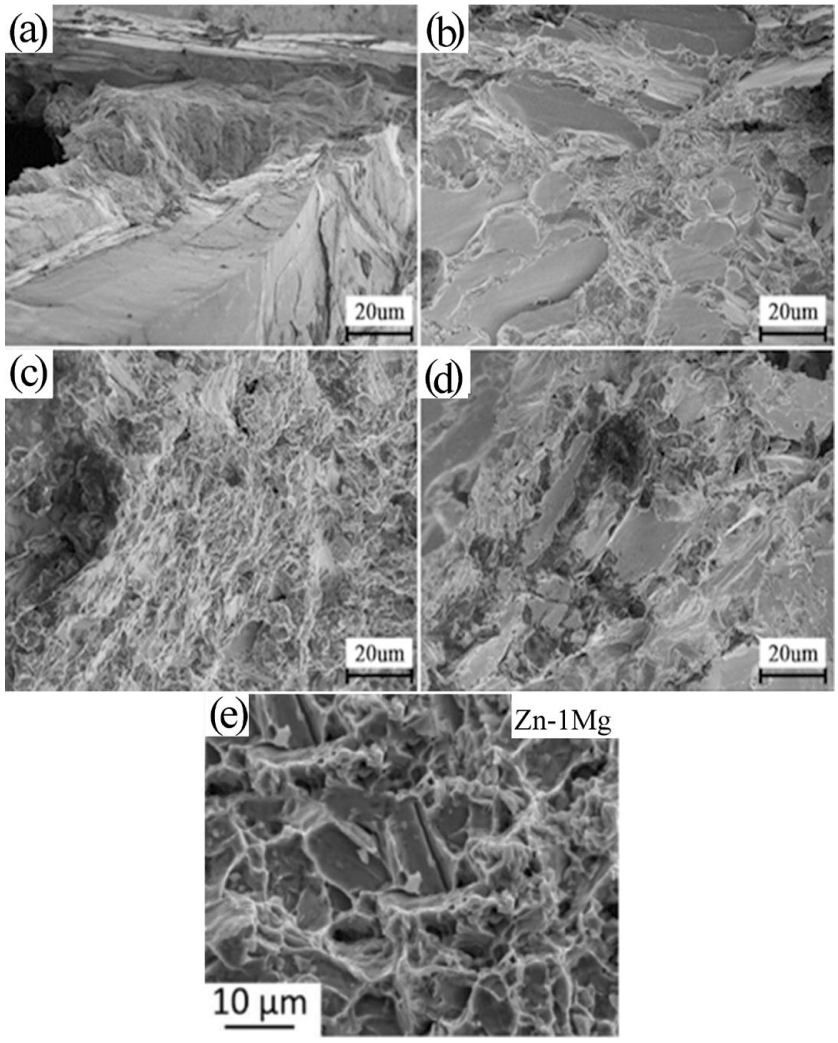

Fig. 3. SEM image of tensile fracture morphology: (a) pure zinc; (b) Zn-1Mg-1.0 wt.% Sn; (c) Zn-1Mg-2.0 wt.% Sn and (d) Zn-1Mg-5.0 wt.% Sn; (e)Zn-1Mg

morphology of pure zinc, Zn-1Mg [32] and as-cast Zn-Mg-xSn alloys. It can be seen from the figure that pure Zn is a typical brittle fracture, and the fractures of Zn-1Mg and Zn-1Mg-xSn alloys have obvious dimples, showing typical ductile fracture characteristics, of which Zn-1Mg-2.0 wt.% Sn alloy dimples pass through the crack interface and are relatively uniform and obvious. Therefore, the tensile properties of Zn-1Mg-2.0 wt.% Sn alloy are better than other metal alloys.

Fig. 4 shows the electrochemical polarization curves of pure zinc and as-cast Zn-1Mg-xSn alloys in SBF solution at 37°C. TABLE 2 shows the electrochemical corrosion properties of pure zinc, Zn-1Mg [6] and as-cast Zn-1Mg-xSn alloys. As the Sn content increases, E_{corr} moves in the negative direction. Both I_{corr} and CR show a trend of rising first and then falling. R_p shows a trend of falling first and then rising. This is because the standard electrode potential of Sn (-0.14 V) is higher than the standard electrode potential of Zn (-0.76 V) and the standard electrode potential of Mg (-2.37 V). Mg_2Zn_{11} and $MgZn_2$ is an intermediate compound formed of Mg and Zn in the Zn-Mg-xSn alloys. The Mg_2Zn_{11} phase contains higher Zn, and the corrosion rate is close to pure zinc, which inhibits the formation of galvanic cells, thereby improving the resistance of the corroded alloy; with the increase of Sn content, the corrosion rate first increases and then decreases. This is because the Mg_2Sn phase and a certain amount of Sn element precipitate at the grain boundaries. Since the standard electrode potential of Sn is higher than that of Zn and Mg, it further increases the occurrence of corrosion and reduces the corrosion resistance of the alloy to a certain extent.

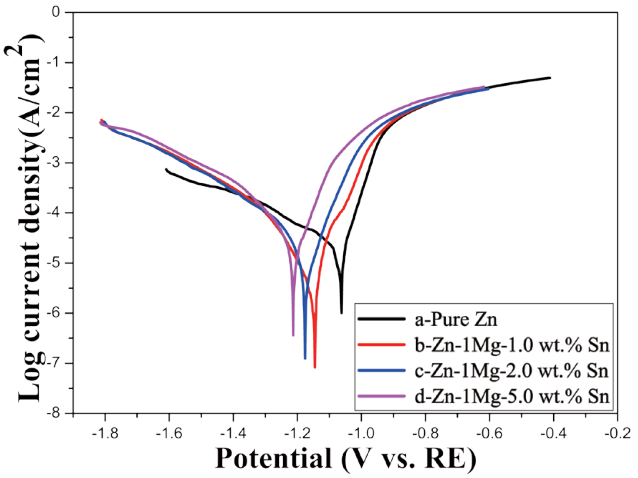

Fig. 4. Tafel polarization curves of pure zinc and Zn-Mg-xSn alloys (a-Pure Zn; b-Zn-1Mg-1.0 wt.% Sn; c-Zn-1Mg-2.0 wt.% Sn; d-Zn-1Mg-5.0 wt.% Sn)

Fig. 5 shows the corrosion rate of pure zinc and as-cast Zn-1Mg-xSn alloys immersed in SBF solution at 37°C for 60 days. It can be seen from the data in the figure that the corrosion rate is not very different when immersed for 7 days. Among them, the corrosion rate of Zn-1Mg-1.0 wt.% Sn is the slowest, and the corrosion rate of pure zinc is the fastest; when immersed for 15 days, the corrosion of Zn-1Mg-2.0 wt.% Sn the rate basically did not change much. The corrosion rate of pure zinc and other metal alloys increased; after 30 days of immersion, the corrosion rate of the immersed sample began to slow down. Among them, the corrosion rate of Zn-1Mg-2.0 wt.% Sn was the smallest, and that of pure zinc and Zn-1Mg-5.0 wt.% Sn has the closest corrosion rate and the largest corrosion rate; after 60 days of immersion, the corrosion rate of the immersed sample increases slightly, among which the corrosion rate of pure zinc and Zn-1Mg-2.0 wt.% Sn are basically the same, and the corrosion rate of Zn-1Mg-5.0 wt.% Sn is the highest.

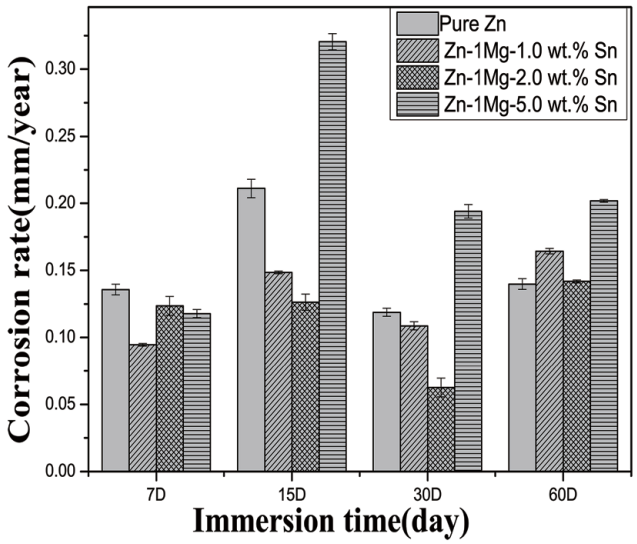

Fig. 5. Corrosion rate of pure zinc and Zn-1Mg-xSn alloys in SBF solution at 37°C

Fig. 6 shows the corrosion morphology of pure zinc and Zn-Mg-xSn alloys immersed in SBF solution at 37°C for 7 days, 15 days, 30 days and 60 days. When immersed for 7 days, the samples were mainly pitted. The pure zinc and Zn-1Mg-1.0 wt.% Sn samples have relatively uniform corrosion pits on the surface, and the corrosion is relatively light. The corrosion of Zn-1Mg-2.0 wt.% Sn and Zn-1Mg-5.0 wt.% Sn is more serious. Corrosion cracks appear; after 15 days of immer-

TABLE 2

Electrochemical corrosion parameters of pure zinc and Zn-1Mg-xSn alloys in SBF solution at 37°C

Materials (wt.%)	E_{corr} (V)	I_{corr} (μA·cm^{-2})	R_p (kΩ·cm^2)	Corrosion rate (mm/year)
Pure Zn	–1.062±0.015	26.57±0.05	0.778±0.007	0.322±0.006
Zn-1Mg-1.0 wt.% Sn	–1.145±0.027	53.68±0.08	0.706±0.005	0.652±0.009
Zn-1Mg-2.0 wt.% Sn	–1.176±0.021	10.32±0.03	1.966±0.012	0.126±0.005
Zn-1Mg-5.0 wt.% Sn	–1.213±0.024	22.19±0.05	0.854±0.009	0.279±0.007
Zn-1Mg [18]	–0.999±0.005	9.94±0.02	1.349±0.006	0.151±0.003

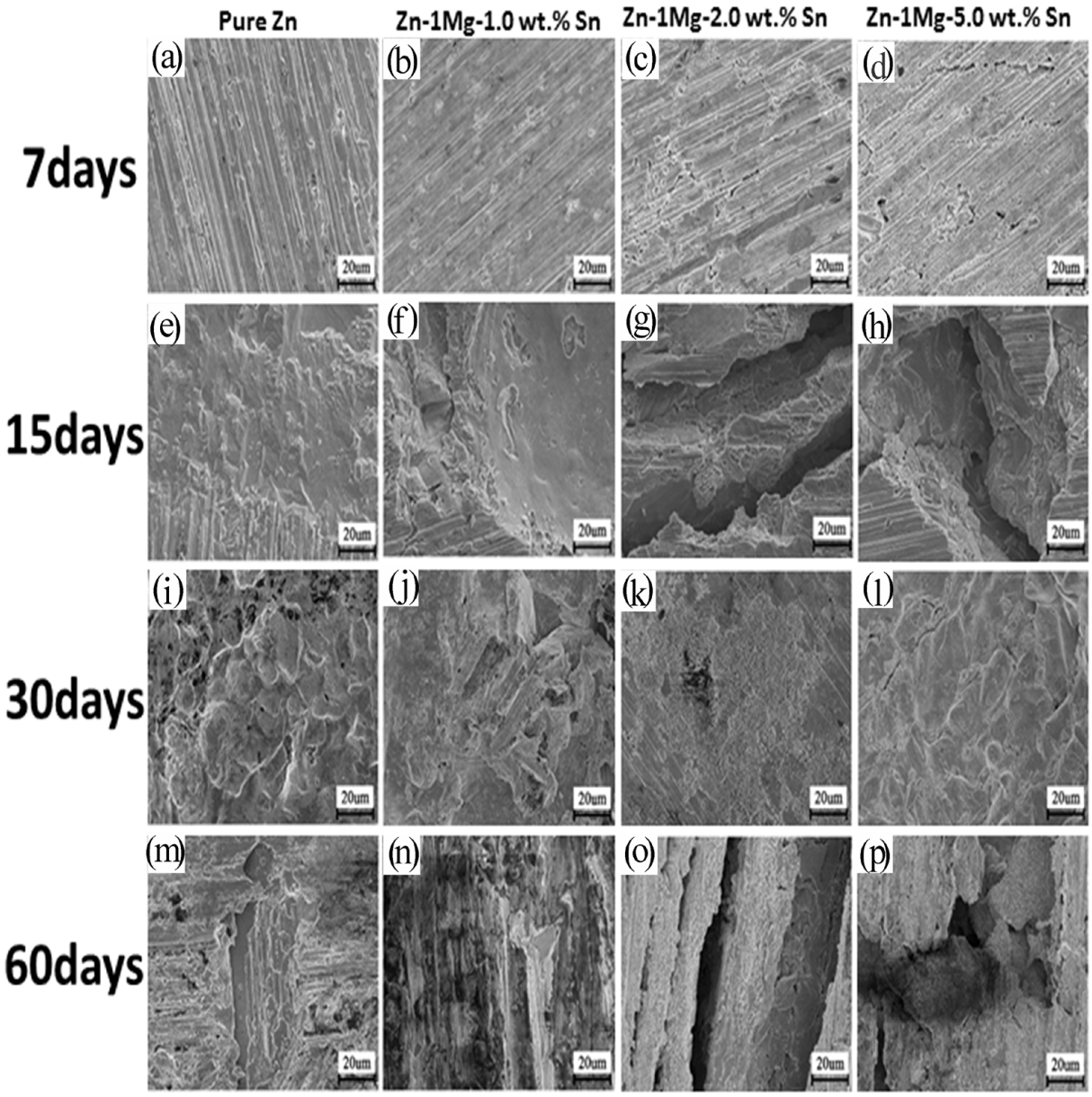

Fig. 6. Corrosion morphology of pure zinc and Zn-1Mg-xSn alloys immersed in SBF solution at 37°C for 7 days: (a) pure zinc; (b) Zn-1Mg-1.0 wt.% Sn; (c) Zn-1Mg-2.0 wt.% Sn and (d) Zn-1Mg-5.0 wt.% Sn; corrosion morphology after immersion for 15 days: (e) pure zinc; (f) Zn-1Mg-1.0 wt.% Sn; (g) Zn-1Mg-2.0 wt.% Sn and (h) Zn-1Mg-5.0 wt.% Sn; corrosion morphology after immersion for 30 days: (i) pure zinc; (j) Zn-1Mg-1.0 wt.% Sn; (k) Zn-1Mg-2.0 wt.% Sn and (l) Zn-1Mg-5.0 wt.% Sn; corrosion morphology after immersion for 60 days: (m) Pure zinc; (n) Zn-1Mg-1.0 wt.% Sn; (o) Zn-1Mg-2.0 wt.% Sn and (p) Zn-1Mg-5.0 wt.% Sn

sion, the surface of pure zinc is still relatively smooth, without corrosion cracks and deep corrosion pits. Increased corrosion for Zn-1Mg-1.0 wt.% Sn compared to pure Zn, but overall it is relatively smoother. There are deeper corrosion pits in the alloy, and the corrosion is more serious. After 30 days of immersion, the surface corrosion of pure zinc increased, and the pitting corrosion continued to expand and turned into surface corrosion. The corrosion degree of Zn-1Mg-1.0 wt.% Sn deepens, and corrosion cracks appear, and the corrosion of Zn-1Mg-2.0 wt.% Sn is deepened, corrosion cracks appear, the corrosion area is enlarged, and the corrosion surface has many larger corrosion pits and particles. The corrosion of Zn-1Mg-5.0 wt.% Sn is the most serious, and some of the alloy matrix appears loose and peeled. After 60 days of immersion, corrosion cracks even appeared on the surface of pure zinc, and Zn-1Mg-1.0 wt.% Sn was corroded, and the cracks became corroded surfaces, and the corrosion was further intensified. Zn-1Mg-2.0 wt.% Sn further aggravated the corrosion along the corrosion cracks, and the surface part of the substrate seemed to fall off. The surface corrosion of Zn-1Mg-5.0 wt.% Sn is further intensified, the base alloy is severely peeled off, and the good corrosion morphology cannot be maintained.

Fig. 7 is a graph of the hemolysis rate of pure zinc and Zn-1Mg-xSn alloys. Experimental results show that the hemolysis rate of pure zinc and Zn-1Mg-xSn alloys are lower than the safety threshold (5%), indicating that pure zinc and Zn-1Mg-xSn alloys will not damage red blood cells during the degradation

process, leaded to severe hemolysis. Compared with pure zinc, the hemolysis rate of Zn-1Mg-1.0 wt.% Sn and Zn-1Mg-2.0 wt.% Sn alloy is significantly reduced and less than the safety threshold (5%) [25], while the hemolysis rate of Zn-1Mg-5.0 wt.% Sn alloy is not much different than that of pure zinc, but is better than that of pure zinc. The hemolysis rate increased with the increase of tin content. This indicates that the precipitation of Mg^{2+} in Zn-1Mg-xSn alloys increases the pH value of the culture dish and destroys the RBC, resulting in an increased hemolysis rate.

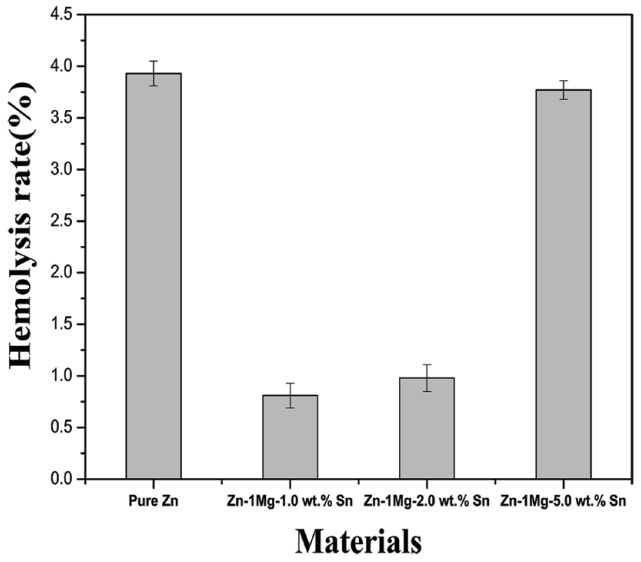

Fig. 7. Hemolysis rate of pure zinc and Zn-1Mg-xSn alloys

Fig. 8 is platelet adhesion morphology between pure zinc, Zn-1Mg [18] and Zn-1Mg-xSn alloys. It is showed that the platelets attached to the surface of pure zinc and Zn-1Mg alloy. Observation indicated no pseudopodia are formed and only a small number of platelets are broken. The number of platelets attached to the surface of Zn-1Mg-1.0 wt.% Sn is very small, and there is no aggregation phenomenon. The number of platelets on the surface of Zn-1Mg-2.0 wt.% Sn is small, there is no aggregation, there is no obvious prosthetic foot, but some platelets are broken. There is no aggregation on the surface of Zn-1Mg-5.0 wt.% Sn, the platelets are in an isolated state, and the morphology changes greatly, but the number of platelets on the surface is very small. The reason is that the precipitation of Mg^{2+} in the Zn-1Mg-xSn alloys result in a significant change in the local pH of the petri dish, resulting in red blood cells due to internal and external cells. Osmotic pressure rises and rupture occurs, leading to hemolysis. It can be seen from the platelet adhesion morphology that with the increase of Sn content, the number of platelets adhering to the surface of the sample increases, and the morphology changes from spherical to dendritic from the beginning. It has found that the number of platelet adhesion is small and no cell ruptures. It has the better blood compatibility and a good hemolysis rate. This may have potential applications in vascular stent materials.

4. Conclusions

In this research, the developed new Zn-1Mg-xSn (x = 0, 1.0, 2.0, 5.0 wt.%) alloys have potential biomedical application. Following conclusions can be drawn:

1. Compared with pure zinc and Zn-1.0 wt.% Mg, the comprehensive mechanical properties of Zn-1Mg-xSn alloys are significantly improved, and with the increase

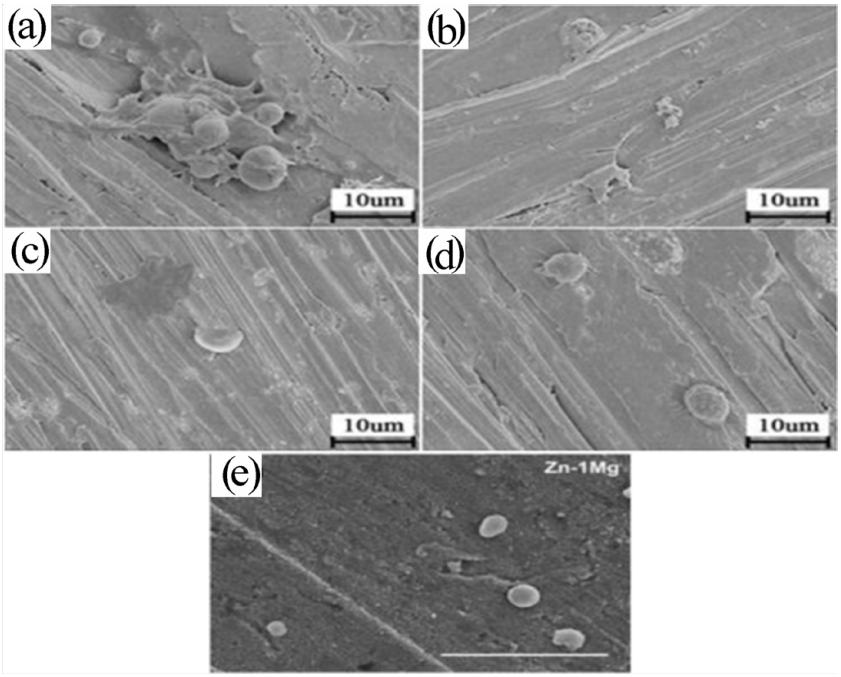

Fig. 8. Platelet adhesion morphology of pure Zn, Zn-1Mg and Zn-1Mg-xSn: (a) Pure Zn; (b) Zn-1Mg-1.0 wt.% Sn; (c) Zn-1Mg-2.0 wt.% Sn; (d) Zn-Mg-5.0 wt.% Sn; (e) Zn-1Mg

of Sn content, the elongation of the alloy increases, and the tensile strength, yield strength and hardness all show a trend of first increasing and then decreasing among them, Zn-1Mg-2.0 wt. % Sn alloy has the best comprehensive mechanical properties. The alloy material has a tensile strength (UTS) of 173.2 ±3.7 MPa, the yield strength (YS) of 120.7 ± 2.4 MPa, an elongation (σ) of 5.64 ± 0.08 % and a hardness of 76.9 ± 0.8 HV.

2. The Zn-1Mg-xSn alloys maintain the ideal degradation rate compared with pure Zn. Platelet adhesion test confirms that the Zn-1Mg-2.0 wt. % Sn alloy hemolysis of rate is only 0.81± 0.02%. It indicates that the Zn-1Mg-xSn alloys has good haemocompatibility.

Acknowledgements

Authors are grateful for the support of experiments works by project China Scholarship Council (CSC 201908450006) under start 2021 program and the Ministry-province jointly-constructed cultivation base for the State Key Laboratory of Processing for Non-ferrous Metal & Featured Materials Foundation.

REFERENCES

[1] E. Gómez-Barrena, P. Rosset, D. Lozano, J. Stanovici, C. Ermthaller, F. Gerbhard, Bone. **70**, 93-101 (2015).
[2] W. Xu, F. Yu, L. Yang, B. Zhang, B. Hou, Y. Li, Mater. Sci. Eng. C-Mater. Biol. Appl. **92**, 11-9 (2018).
[3] D.P. Zhao, Y.K. Chen, K.K. Chang, T. Ebel, F. Pyczak, Trans. Nonferrous Met. Soc. China. **28**, 1342-50 (2018).
[4] A. Bekmurzayeva, W.J. Duncanson, H.S. Azevedo, D. Kanayeva, Mater. Sci. Eng. C-Mater. Biol. Appl. **93**, 1073-89 (2018).
[5] K. Yamanaka, M. Mori, I. Kartika, M.S. Anwar, K. Kuramoto, S. Sato, A. Chiba, Corrosion Sci. **148**, 178-87 (2019).
[6] Y. Zheng, Y. Wu, Acta Metall. Sin. **53**, 257-97 (2017).
[7] M. Ridzwan, S. Solehuddin, A.Y. Hassan, A.A. Shokri, M. Ibrahim, J. Med. Sci. **7**, 460-7 (2007).
[8] H. Li, Y. Zheng, L. Qin, Prog. Nat. Sci. **24**, 414-22 (2014).
[9] Y. Zhang, Y. Yan, X. Xu, Y. Lu, L. Chen, D. Li, Y. Dai, Y. Kang, K. Yu, Mater. Sci. Eng. C-Mater. Biol. Appl. **99**, 1021-34 (2019).
[10] W.R. Zhou, Y.F. Zheng, M.A. Leeflang, J. Zhou, Acta Biomater. **9**, 8488-98 (2013).
[11] Y.F. Zheng, X.N. Gu, F. Witte, Mater. Sci. Eng. R-Rep. **77**, 1-34 (2014).
[12] Q. Chen, G.A. Thouas, Mater. Sci. Eng. R-Rep. **87**, 1-57 (2015).
[13] H.M. Ledbetter, J. Phys. Chem. Ref. Data. **6**, 1181-203 (1977).
[14] S.I. Katsumata, R. Katsumata-Tsuboi, M. Uehara, K. Suzuki, J. Nutr. **139**, 238-43 (2009).
[15] J. Aaseth, G. Boivin, O. Andersen, J. Trace Elem. Med. Biol. **26**, 149-52 (2012).
[16] R. Zhang, P. Lee, V.C. Lui, Y. Chen, X. Liu, C.N. Lok, M. To, K.W. Yeung, K.K. Wong, Nanomedicine. **11**, 1949-59 (2015).
[17] Z. Tang, H. Huang, J. Niu, L. Zhang, H. Zhang, J. Pei, J. Tan, G. Yuan, Mater. Des. **117**, 84-94 (2017).
[18] H.F. Li, X.H. Xie, Y.F. Zheng, Y. Cong, F.Y. Zhou, K.J. Qiu, X. Wang, S.H. Chen, L. Huang, L. Tian, L. Qin, Sci. Rep. **5**, 10719 (2015).
[19] P.K. Bowen, J. Drelich, J. Goldman, Adv. Mater. **25**, 2577-82 (2013).
[20] D. Vojtech, J. Kubasek, J. Serak, P. Novak, Acta Biomater. **7**, 3515-22 (2011).
[21] H. Guo, Y. He, Y. Zheng, Y. Cui, Mater. Lett. **275**, 128190 (2020).
[22] S. Zhao, C.T. Mcnamara, P.K. Bowen, N. Verhun, J.P. Braykovich, J. Goldman, J.W. Drelich, Metall. Mater. Trans. A-Phys. Metall. Mater. Sci. **48**, 1204-15 (2017).
[23] H. Yang, B. Jia, Z. Zhang, X. Qu, G. Li, W. Lin, D. Zhu, K. Dai, Y. Zheng, Nat. Commun. **11**, 401 (2020).
[24] C. Xiao, L. Wang, Y. Ren, S. Sun, E. Zhang, C. Yan, Q. Liu, X. Sun, F. Shou, J. Duan, H. Wang, G. Qin, J. Mater. Sci. Technol. **34**, 1618-27 (2018).
[25] J.L. Aschner, M. Aschner, Mol. Asp. **26**, 353-62 (2005).
[26] D. Chen, Y.P. Ren, Y. Guo, W.L. Pei, H.D. Zhao, G.W. Qin, Trans. Nonferrous Met. Soc. China. **20**, 1321-5 (2010).
[27] C. Zhao, F. Pan, Z. Shuang, H. Pan, S. Kai, A. Tang, A. Tang, Mater. Sci. Eng. C-Biomimetic Supramol. Syst. **54**, 245-51 (2015).
[28] J. Kubasek, D. Vojtech, J. Lipov, T. Ruml, Mater. Sci. Eng. C-Biomimetic Supramol. Syst. **33**, 2421-32 (2013).
[29] F.G. Meng, J. Wang, L.B. Liu, Z.P. Jin, J. Alloy. Compd. **508**, 570-81 (2010).
[30] T. Kokubo, H. Takadama, Biomaterials. **27**, 2907-15 (2006).
[31] H. Gong, K. Wang, R. Strich, J.G. Zhou, Biomed. Mater. Res. Part B. **103**, 1632-40 (2015).
[32] C. Garcia-Mintegui, L.C. Cordoba, J. Buxadera-Palomero, A. Marquina, E. Jimenez-Pique, M.P. Ginebra, J.L. Cortina, M. Pegueroles, Bioact. Mater. **6**, 4430-46 (2021).